Global and local mobility as a barometer for COVID-19 dynamics

Kevin Linka[1], Alain Goriely[2], Ellen Kuhl[1*]

[1]Mechanical Engineering, Stanford University, USA
[2]Mathematical Institute, Oxford University, UK

*To whom correspondence should be addressed; E-mail: ekuhl@stanford.edu.

The spreading of infectious diseases including COVID-19 depends on human interactions. In an environment where behavioral patterns and physical contacts are constantly evolving according to new governmental regulations, measuring these interactions is a major challenge. Mobility has emerged as an indicator for human activity and, implicitly, for human interactions. Here we study the coupling between mobility and COVID-19 dynamics and show that variations in global air traffic and local car traffic mobility can be used to stratify different disease phases. Our study shows that, for 26 European countries, maximal correlation between driving mobility and disease dynamics follows a normal distribution with a 17-day mean and two-day standard deviation. Our findings suggests that local mobility can serve as a quantitative metric to forecast future reproduction numbers and identify the final stages of the pandemic when mobility and reproduction become decorrelated.

Introduction

A barometer is an instrument that measures air pressure. Its main purpose is to forecast short term changes in the weather. It is often imprecise as it relies on a number of assumptions linking variations of air pressure to atmospheric conditions. Nonetheless, overall, we accept it as an important tool in weather prediction that has saved countless

lives since its introduction for forecasting in the 19th century. In an evolving crisis like the COVID-19 pandemic, the world is in a dire need of a barometer that would provide us with reliable estimates of the disease dynamics when lockdown measures are either enacted or removed.

The transmission of an infectious disease depends mostly on three key aspects: the biology of the disease when individuals are in contact, social and human behavior that dictate the way individuals interact, and the physics of such contacts (closed spaces, close contact, crowded spaces) (*1, 2*). We still do not know about the details of the COVID-19 pathology, and in particular how different age or population groups either transmit or are susceptible to the disease (*3, 4*). But, the disease pathogenicity and transmissibility cannot be altered in the absence of a vaccine or preventive treatments. On the behavioral side, there has been a dramatic change in everyday habits with widespread adoption of new rules to prevent both close contact between individuals and the exchange of contaminated bodily fluids. The remaining factors, frequency and type of contact, depend on human activity. Work, school, and leisure inevitably increase the number of contacts, and hence the risk of transmission that occurs in everyday life (*5*). At the global level, human mobility, tracked by mobile phone use, has recently emerged as a possible proxy for human activity. Studies of the effective reproduction number $R(t)$, the average number of secondary infections caused by an infected person, against in-state human mobility data in China (*6–8*) and in the United States (*9, 10*) have demonstrated that as long as the epidemic is ongoing, mobility and reproduction number are indeed correlated (*11*). Interestingly, successful exit strategies reveal a decorrelation between these mobility and reproduction which implies that an increase in activity does not lead to an increase in infection.

When considered together, current mobility data and disease indicators follow the typical pattern shown in Fig. 1(a) with four distinct phases: Phase I of exponential growth during the initial outbreak of the disease; Phase II of outbreak control during which global and local mobility are rapidly reduced; Phase III of reduced growth under lockdown with reduced local and global mobility; and Phase IV of gradual exit during which lockdown measures are successively released and mobility increases while the number of new cases continues to decrease. An important feature of the outbreak dynamics is that a reduction in the number of new cases is delayed by about two weeks compared to the reduction in mobility and that this feature appears systematically in across countries. This is not particularly surprising as it is the primary goal of lockdown measures. However, we will show that another key property of the data is the high correlation between mobility data and the reproduction number *after* lockdown. We can formally exploit this property to understand the effects of human activity on the reproduction number.

Modeling has proven to be a key element to understand disease dynamics (*12, 13*)

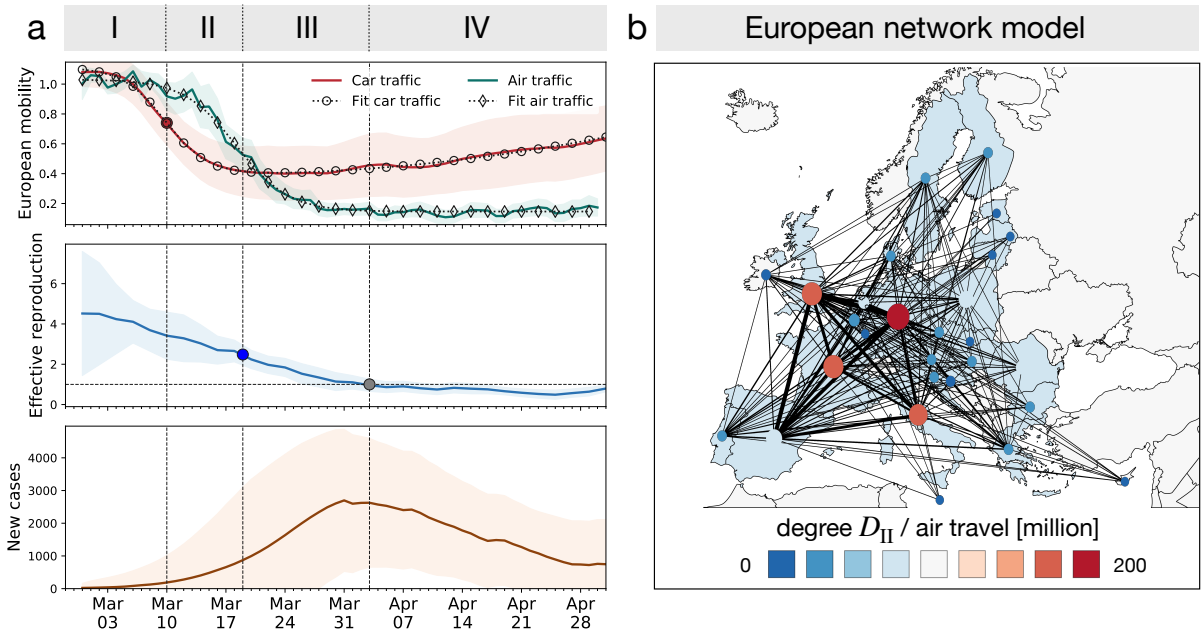

Figure 1: **Phases of the COVID-19 outbreak in terms of of global and local mobility, reproduction number, and reported cases.** (a) Solid lines are the mean values of all considered countries, shaded areas correspond to the standard deviation. Phase I is the phase of exponential growth during the initial outbreak of the disease. Phase II is the phase of outbreak control during which global and local mobility are rapidly reduced. Phase III is the phase of reduced growth under lockdown with reduced local and global mobility. Phase IV is the phase of gradual exit during which lockdown measures are successively released and mobility increases while the number of new cases continues to decrease. The effective reproduction number $R(t)$ does not return to its initial value since many behavioral changes are still in place. The absolute and relative magnitudes of the five phases depend on the individual social and political organizations of each geographic entity, state or country. The model parameters of the global mobility model (left): $y_0 = 1$, $t^* = 25.2$,$T = 6.14$, $P(t) = 0.15$. For the local mobility model (right) are $y_0 = 1.12$, $t^* = 16.7$, $T = 4.9$, $P(t) = 10^{-4}\,t^2 - 5.7 \cdot 10^{-3}\,t + 0.47$. (b) Global mobility network of European countries with 26 nodes and the 201 most traveled edges.

and establish new public health policies (*14*). While most models rely on standard population models such as the SEIR model, there are many refinements and variations that take into account contact between different groups, susceptibility, the effect of air travel through networks, and the effect of testing and lockdown (*14, 15*). These models can be deterministic, representing average quantities, or stochastic, associated with uncertainties in data and disease dynamics. Due to the large uncertainties associated with model parameters, most of the actual work consists in devising appropriate statistical methods to infer parameters from incomplete data. This process naturally generates confidence intervals for any prediction based on these models. Precise predictions require more

fine-grained models (*16*). These models consider multiple effects and mirror the complexity of interaction in societies; they include many parameters, including mobility and proximity data, that are difficult to track, especially since rapid changes in behavior often render a-few-day-old studies and historic trends irrelevant.

A complementary approach is to consider coarse-grained models with fewer parameters. While these models cannot be used to make precise long-term predictions of the number of infections or deaths on a given day, they are particularly valuable when predicting global trends in a robust manner since they only rely on a few parameters that are almost entirely determined by the data alone. Here, we adopt this approach to study the relation between mobility and disease dynamics. We use the well-established SEIR (Susceptible - Exposed - Infectious - Recovered) compartment model with a network structure and evaluate the local disease dynamics at the level of a node, which represents an individual country. We incorporate the local driving mobility at the nodal level and the global mobility at the network level through passenger air travel with diffusive transport. To take full advantage of prior knowledge about the model parameters and the available data of each country, we combine our network model with a hierarchical Bayesian parameter inference and apply Markov Chain Monte Carlo sampling to obtain posterior distributions to our model uncertainties.

Results

Reduced mobility drastically reduces the effective reproduction number– Figure 2 shows the change in air and car traffic starting February 15. Each dot represents the day at which the corresponding country reached 100 or more cases. We notice that different countries share the same overall dynamics: an initial plateau followed by a sudden drop in air traffic and a rapid drop in car traffic followed by a gradual increase. The data reveal three interesting trends. First, local mobility decreases before global mobility with minima in the week of March 17-24 for car and March 24-31 for air traffic. Second, many countries experience a dramatic reduction of mobility, it seems almost voluntary, *before* the national outbreak becomes apparent. Third, there is a clear South-North divide in reduction of local mobility with Spain and Italy experiencing the largest reduction and Sweden and Finland the smallest.

Increased mobility does not notably increase the effective reproduction number– Figures 2(a & b) shows, side by side, the weekly average of driving mobility and the effective reproduction number extracted from the network model. At the early phase of the outbreak, this heatmap shows that a reduction of driving mobility

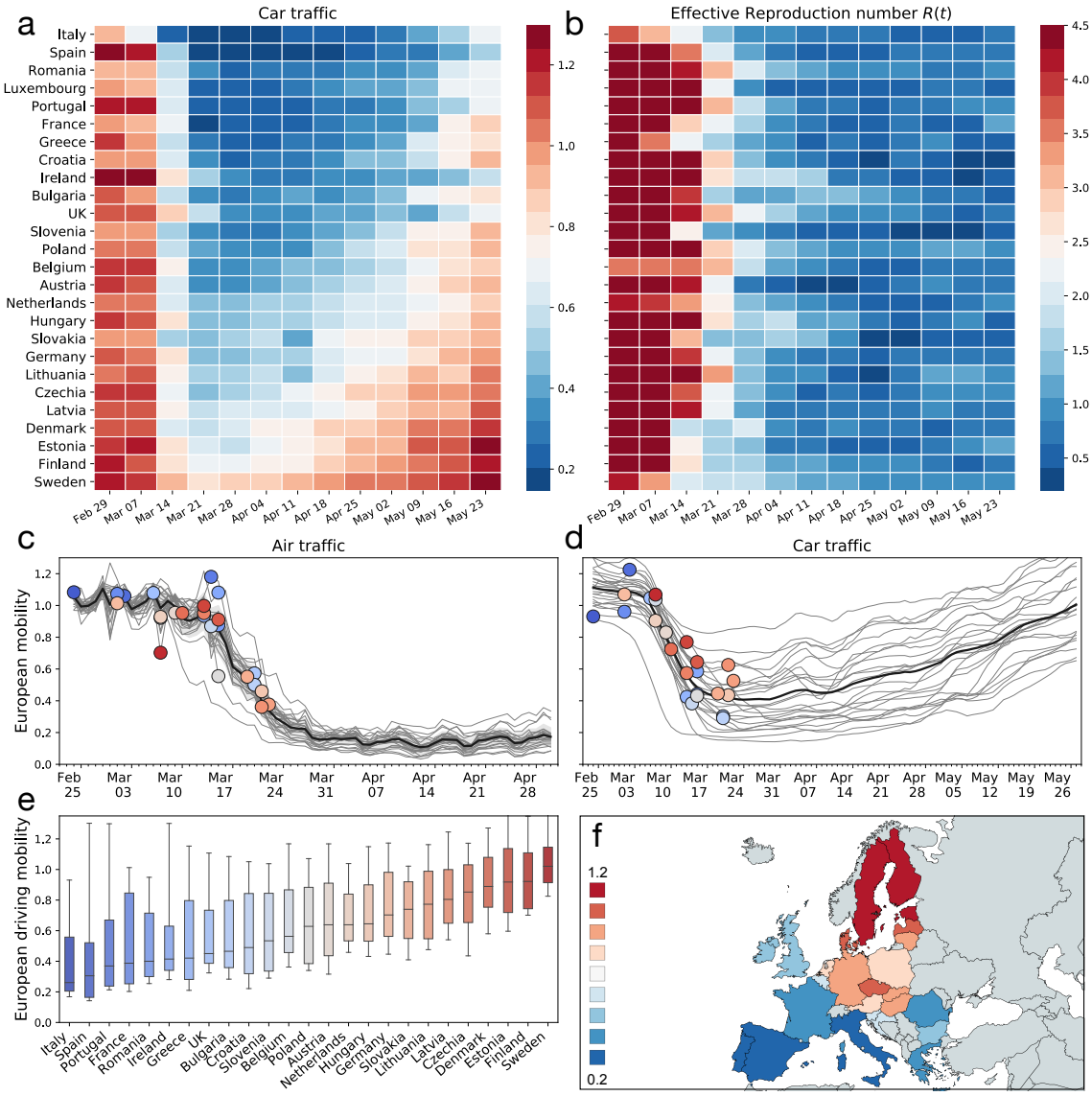

Figure 2: **Global and local mobility across Europe.** (a & b) Weekly average local mobility and effective reproduction number across Europe. (c) Air traffic dropped to 10%±5% from March 13 to March 30. (d) Car traffic dropped to 40%±18% from March 5 to March 17. The dots represent the time point the associated with more than 100 reported cases; the color code indicates the reduction in local mobility, with the largest reduction in Italy and Spain to 26% and 27% and the smallest reduction in Finland and Sweden to 96% and 98%. (e) The box plots show the statistics of the individual driving mobility curves over the depicted time range. (f) The color code represents the change in driving mobility across Europe.

is followed by a reduction of the effective reproduction number with a typical delay of about two weeks. At the later phases, however, an increase in driving mobility in

response to a gradual exit from lockdown does not initiate an increase in the effective reproduction number. This lack of symmetry between reduction and increase of mobility suggests that some other non-pharmaceutical interventions that were adopted in that period may have taken a more prominent role in controlling the effective reproduction number.

Local mobility is highly correlated with the reproduction number– Following the suggestion of Fig. 2(a & b) that there is an association between mobility and disease dynamics, we show in Fig. 3 the evolution of both local mobility and effective reproduction number for all countries that had at least 100 cases on March 10. To ensure similar initial conditions, we begin each simulation at the individual date the country hit 100 confirmed cases. We compute the effective reproduction number, $R(t)$, by the semi-parametric Gaussian process model and use only the country-specific mobility data over time as input. We train the Gaussian process model in a hierarchical manner and share the priors for the model between all countries. The close agreement of the fit in Fig. 3 indicates that the model is capable of learning the individual behavior based on shared posteriors. The hierarchical posterior distribution of the adaption time t^* in Fig. 3 shows a mean response delay of 17 ± 2.0 days, with regional variations ranging from 9.9 days in Austria to 25.2 days in Sweden. We also determined the associated cross-correlation between the local mobility and the effective reproduction number. The averaged time delay over the complete time period results in Δt of 17.7 ± 5.4 days and varies from 12 and 13 days in Spain and Austria to 26 and 28 days in Denmark and Sweden, see Fig 4(a). In addition, to study correlations for different time windows, we successively shorten the considered time interval by five days beginning at the individual start date, the day of 100 reported cases, up to 30 days. For an interval reduction of 30 days, we find an elongation of the delay time up to 28.7 ± 13 days, followed by a decorrelation of local mobility and effective reproduction number, see Fig. 4(b).

Mobility and reproduction number define disease staging– We can now combine both global and local mobility data together with the effective reproduction number to define typical staging dynamics. In Fig. 1, we use a network model for global mobility coupled with the local mobility data at each node. Following the disease outbreak in phase I, the first transition occurs following a drop in local mobility associated with changes in behavior such as working at home or limit on gatherings, and corresponds to an inflection point in the local mobility curve. In most countries, governmental outbreak control and some level of lockdown were established during the following phase II, see Fig. S1(b). The second transition occurs when, similarly, air traffic drops with its corresponding inflection point. During phase III, there is a

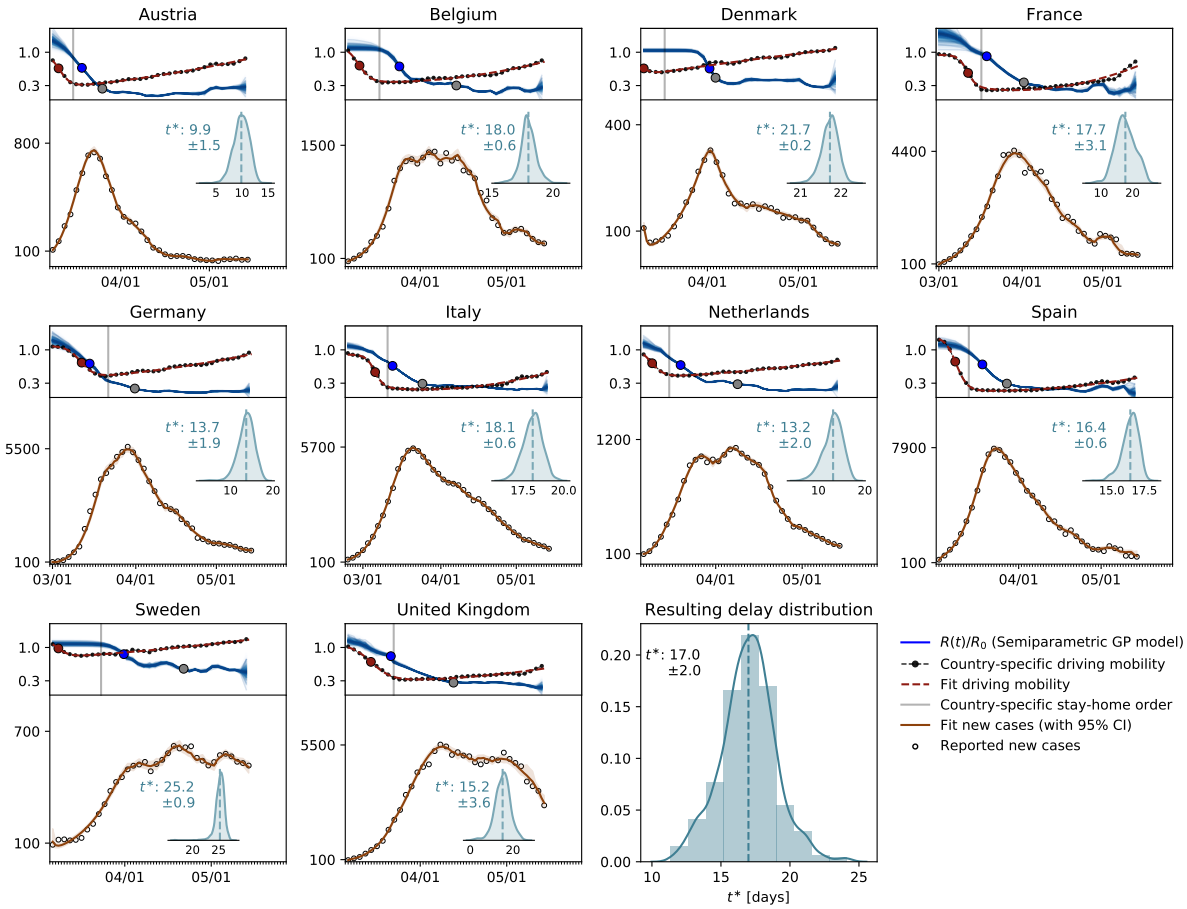

Figure 3: **Local mobility, reproduction number, and reported cases across Europe.** The hierarchical model learns the time-varying effective reproduction number $R(t)$ (blue curve) from the reported cases (black circles) and simulated cases (orange curve) for varying adaptation times t^*. The dots in the top plots indicate the adaptations times t^* of local mobility and reproduction, respectively. The gray dots on the effective reproduction curves highlight the time point each country hit $R(t) = 1$.

slow increase in local mobility but a decrease in the overall reproduction number. The third transition between phases III and IV corresponds to the peak of the number of new cases. After this transition, in phase IV, the reproduction number remains low despite a gradual increase in mobility, resulting in a noticeable reduction of new active cases.

Mobility data can be used to forecast reproduction– The observed high correlation between mobility data and the effective reproduction number, with a typical delay of around 14 days, suggests that we can use mobility data as a barometer for the reproduction

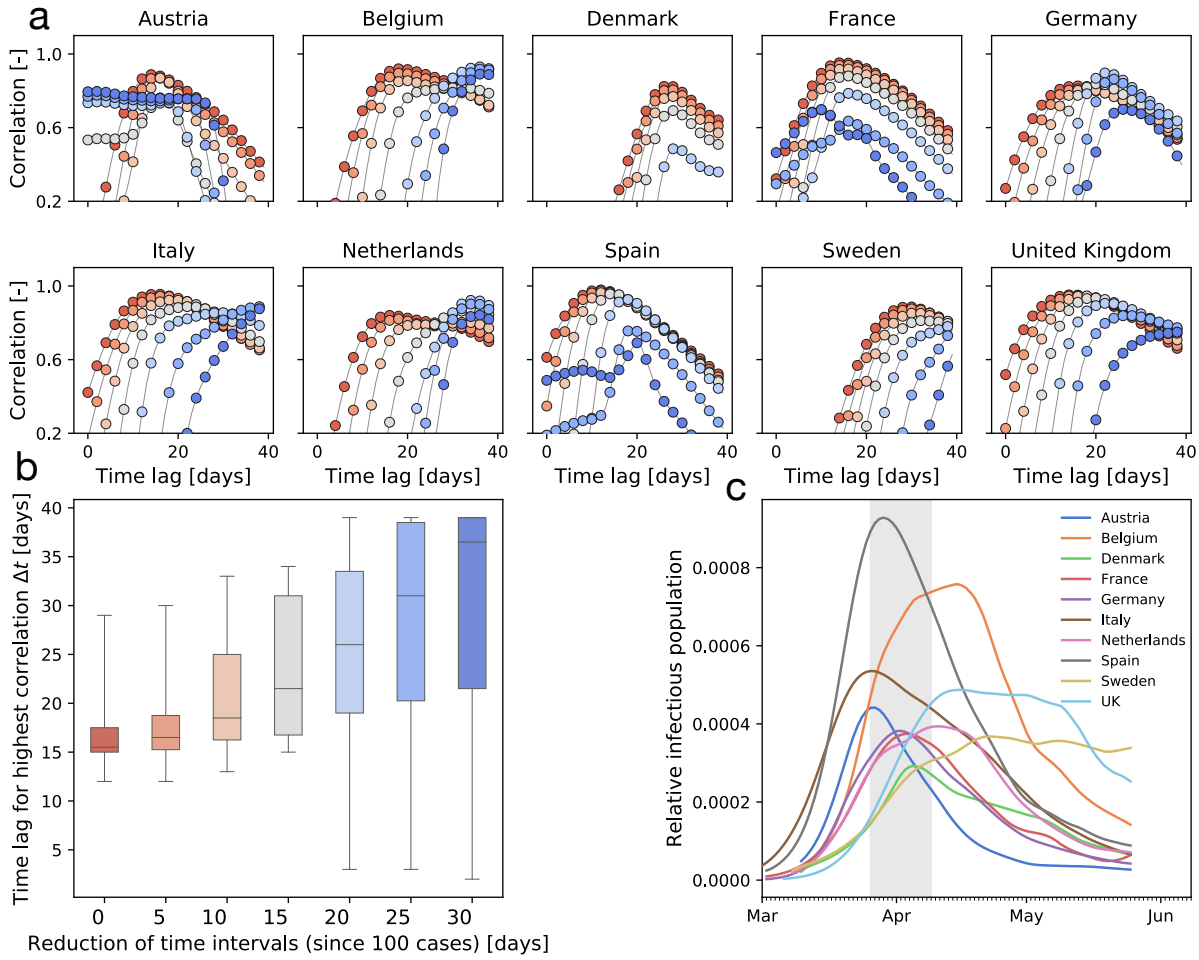

Figure 4: **Cross-correlation between effective reproduction and local mobility for different time intervals.** (a) The panels shows the correlations vs. time lags for seven different time intervals for ten European countries. The color-code represents the different time intervals as indicated for the box plots (b). The box plots visualize the statistics of the highest time lag correlations for the ten countries in seven different time intervals. (c) The curves illustrate the relative infectious population for the ten countries. The gray band highlights the time points where the time intervals starts for a reduction of 30 days.

number. In Fig. 5 we show two different training scenarios where we tested the prediction for the 14 days from April 19 to May 2 for Germany and the UK. In the first scenario, we used data from February 28 until April 19 for training. This period includes a rapid change in car traffic and the implementation of several different control strategies. The second period starts at the point where local mobility is close to a minimum in Europe, therefore we included case data after March 25 into the training dataset. We observe that,

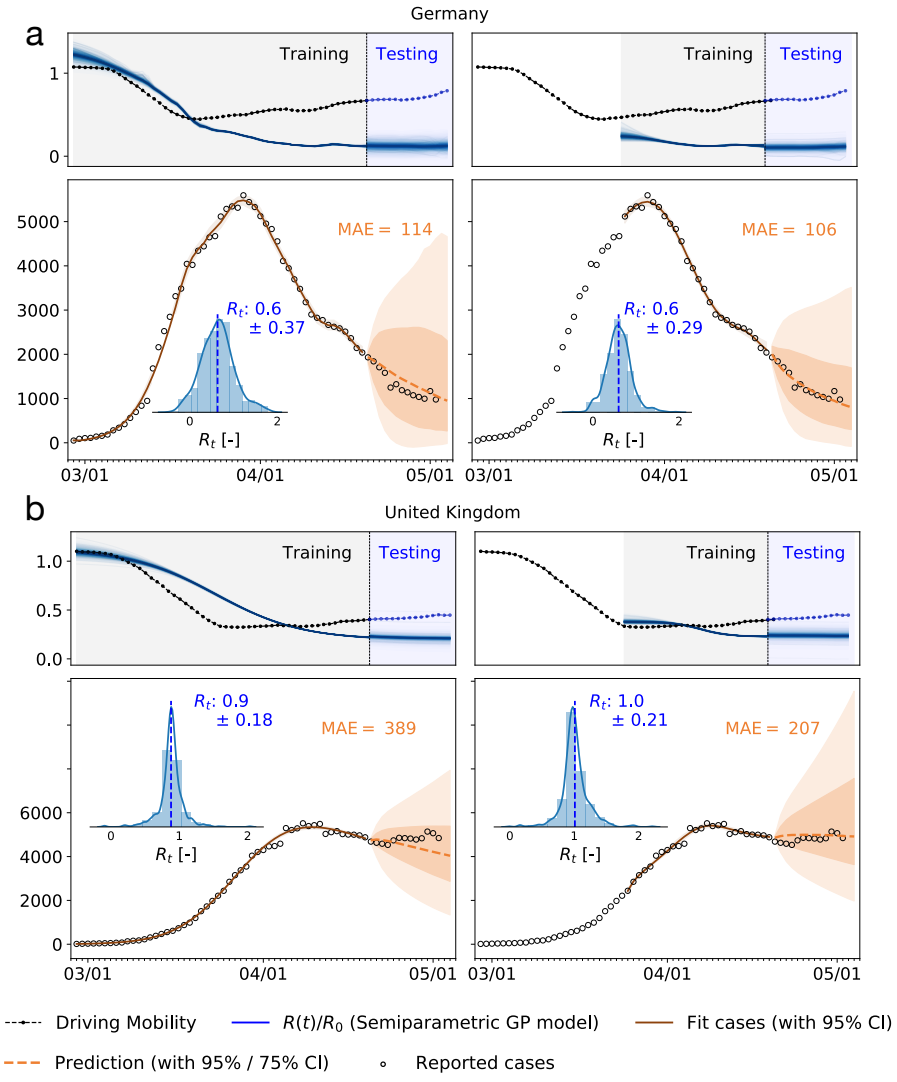

Figure 5: **14-day forecasting of new cases for (a) Germany and (b) United Kingdom.** Both models are trained on the full data set and on the data points after the mobility break down. The histograms show the posterior distributions of the last time step of the predicted effective reproduction number $R(t)$. The orange zones indicate the 95% and 75% confidence intervals and the associated mean absolute errors (MAEs) for the two-week forecasting.

despite the fact that a smaller training set is used, the model prediction for the effective reproduction number is better and fully captures the reproduction dynamics. Figure S2 demonstrates this predictive capabilities of the model for all ten countries.

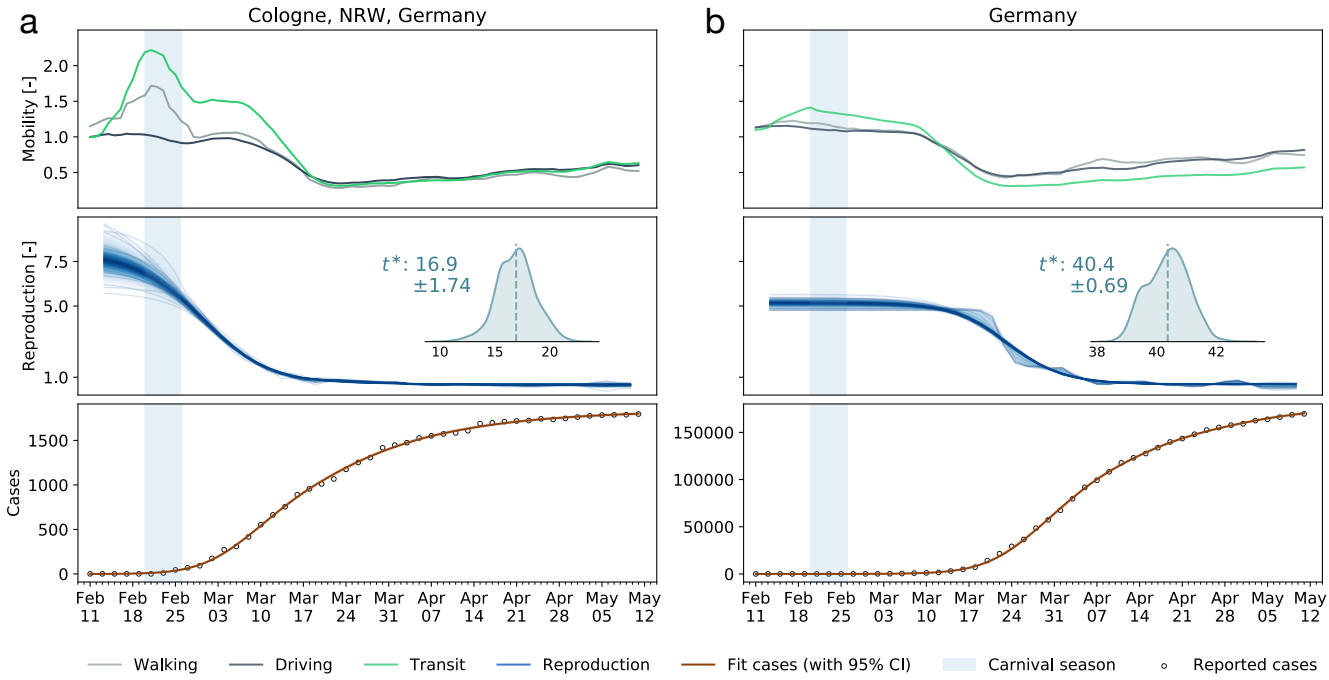

Figure 6: **Dynamics of a super-spreading event.** (a) The Heinsberg Carnival took place between February 20 and 26 (shaded region) and is associated with a large spike in mobility data in the nearby city of Cologne. (b) It is correlated with a local increase of the reproduction number in Cologne, approximately 17 days delayed, and a national increase, approximately 40 days delayed.

Local mobility data can be used to identify possible super-spreading events– Super-spreading events are characterized by a local outbreak when a large population comes in close contact for a significant period of time. Examples includes sporting events, parades, festivals, religious ceremonies, and carnivals. Unavoidably, these events are associated with large population movement and can be captured by mobility data. For instance, the Carnival season between February 20 and 26 in the Heinsberg district drew large crowds and it is believed to be the first COVID-19 hotspot in Germany (*17*). Figure 6 shows the mobility data of the city of Cologne, approximately 70km from Heinsberg. The spike in mobility is directly followed by the epidemic outbreak and correlated with a

change in the reproduction number with a time-delay of 17 days. This highly-localized event rippled across the entire country with a time-delay of about 40 days.

Discussion

The objective of this study was to explore to which extent global and local mobility are correlated with the effective reproduction number, and, accordingly, with the local outbreak dynamics. Using passenger air travel, cell phone mobility data, and reported COVID-19 cases across Europe, we showed that mobility and reproduction are correlated during the early stages of the outbreak, but become decorrelated during later stages. Interestingly, our study identified four distinct phases of the outbreak across all European countries that implemented political counter measures.

Phase 0: During the early stages of the pandemic, global mobility modulates the initial outbreak pattern– Various studies have shown that there is a close correlation between mobility and spreading of infectious disease. For instance, the early pattern of COVID-19 closely mimics passenger air travel (*18*). Global mobility is key to seed the disease in new locations before its local growth. Tight travel restrictions and border control, first implemented in the United States, and then in the entire European Union, mark the end of this phase in Mid March. In response, air travel within the European Union dropped by 95% within less than two weeks. Yet, it becomes clear now that most travel restrictions were implemented too late to protect any country from a local outbreak of COVID-19.

Phase I: Once a location is hit by the pandemic, exponential growth governs the local outbreak dynamics– After local seeding, the outbreak dynamics become decorrelated from global mobility. Instead, the local number of cases increases rapidly and the question of health care resources becomes the focal point in political decision making. At this point, without any additional measures, the outbreak would naturally peak and decay towards the endemic equilibrium (*25*). The timing of the peak, its magnitude, and condition of herd immunity are determined by the basic reproduction number (*20*). For COVID-19, the basic reproduction number R_0 is on the order of three to six (*19*), for which models would predict a peak of active cases from 21% to 39% of the population, occurring between days 46 and 23, and herd immunity after 67% to 86% of the population have become infected.

Phase II: Outbreak control modulates the effective reproduction number by reducing local mobility– To stop the period of exponential growth, political measures,

including local lockdown and limit to gatherings, have been implemented in almost all European countries to limit contact between infectious and susceptible individuals. The rapid reduction of car traffic to 40±21% within less than two weeks in early March is an indicator for a successful contact reduction. Strikingly, in most countries, this reduction in mobility emerged *naturally*, well ahead of political intervention, as a result of voluntary behavioral changes in the population, see Fig. 2.

Phase III: Reduced mobility reduces the number of new cases and initiates a flattening of the curve–In the outbreak dynamics, reduced local mobility induces a reduction of the effective reproduction number R_{t} and with it convergence to an enforced equilibrium state, a converged state under given constraints, long before herd immunity is achieved in the entire population. The speed and magnitude by which the reproduction number drops are a measure of the effectiveness of public health interventions. For example, in Austria, a country that is known for its strict response to the pandemic R_t dropped from 4.0 to 1.1 in only 16 days; in Sweden, a country that implemented relatively lose public restrictions it dropped from 2.0 to 1.1 in as much as 33 days. In the hypothetical case of complete lockdown, the number of new cases, and with it the effective reproduction number, would go to zero. However, Fig. S1(b) shows that even under the strict political constraints imposed in most European countries, the average duration from the point a country hit 100 cases until the reproduction number went down to one is 38 ± 8 days. As long as R_t remains lower than one, the number of new cases continues to decrease, although gradually.

Phase IV: The gradual exit from lockdown reveals the effect of social learning–Following a period of rigorous lockdown, most European governments have begun to slowly relax the strict measures to reduce movement and contacts. This relaxation is clearly reflected in the mobility data in Fig. 2 as a slow increase of local mobility. Two important features are now becoming apparent: First, there is an asymmetry in the decrease and increase of the reproduction number before and after lockdown that can be attributed to social learning and soft political intervention including face masks, physical distancing, and no large gatherings. Second, variations in the reproduction number during the early phases are highly correlated with changes in local mobility, while later they are not. Our analysis with training and testing suggests that, as long as the disease remains endemic, *trends in local mobility allow us to forecast the outbreak dynamics for a two weeks window.* This correlation has potentially important consequences: Some proposed exit strategies suggest either periodic or on-demand lockdown once the number of new cases begins to rise again. The general objective of most outbreak control strategies is to

keep the effective reproduction number either strictly below one or slightly above. The problem with the latter approach is that by the time a critical rise becomes observable, the inertia of the exponential dynamics is already difficult to control and long periods of lockdown would become necessary to manage the overall outbreak dynamics. Our study shows that mobility data can serve as a barometer to adjust particular sectors of the economy, in real time, to maintain *future* effective reproduction numbers smaller than one. Importantly, in this approach, the forecast of the reproduction number, the correlation levels, and the window of correlation can be updated daily as new data become available.

Phase V: Complete decorrelation between mobility and reproduction indicates the end of the pandemic–In the case of COVID-19, during the early stages of exponential growth, almost all European countries experienced a strong reduction in local mobility. Around Mid March, numerous political measures were implemented in different stages, ranging from prohibiting gatherings to complete lockdown, with a restriction to essential business only. During this period, the virus spread non-linearly across Europe, see Fig. 3 and Fig. 4(c). Throughout this time window, individual mobility had a massive potential to accelerate the outbreak and generate large effective reproduction numbers. This agrees well with our observation of a distinct time lag and associated strong correlations between mobility and reproduction among all European countries within the full dataset, see Fig. 4(a). Due to behavioral changes after the first phase of the outbreak, our analysis suggests that the time lag increased from initially 17.7±5.4 to 28.7±13 days, before mobility and reproduction decorrelate. This is clearly visible in the cross-correlation for different time intervals of the dataset, see Fig. 4(a & b). The decorrelation begins after the infectious curve peaked, i.e., $R(t) \leq 1$, and the dynamics of traffic and reproduction become increasingly independent as the effective reproduction approaches zero. In this range, the amount of infectious individuals is too low to be amplified by human mobility. For example, for the case of Austria, which was among the first countries in Europe to aggressively implement outbreak control, we observe an early peak at the end of April in Fig. 4(c). Austria was one of the first countries worldwide to report an effective reproduction number below one, which resulted in an early decorrelation and a vanishing distinct time shift between local mobility and reproduction, see Fig 4(a). The effect of decorrelation at low new case numbers is inherently built into our model: The latent variable formulation of the effective reproduction number, as a function of local mobility within the SEIR model, become increasingly less sensitive to mobility changes for a low infectious population. At the same time, it remains specific enough to capture mobility spikes as we can see for the example of France in Fig. S2.

Taken together, the strong correlation between mobility and reproduction in the endemic phase, and the loss of correlation in the later phases, suggest that mobility is a reliable predictor of to predict outbreak dynamics. Our study suggests that biweekly mobility trends can be used to stratify different phases of the pandemic, identify super-spreading events, and guide political decision making. Mobility is a suitable pandemic barometer.

Methods

The foundation of our modeling methodology, to account for human activity at different scales, is the standard SEIR (Susceptible - Exposed - Infectious - Recovered) compartment model. We model the inter-country specific outbreak dynamics using a network of passenger air travel between individual countries, combined with the local driving mobility at the nodal level. To account for our prior knowledge of the model parameters and the available data for each country, we combine our network model with a hierarchical Bayesian parameter inference by applying Markov Chain Monte Carlo sampling to obtain posterior distributions for uncertainty quantification.

COVID-19 outbreak data, global and local mobility

We draw the COVID-19 outbreak data for 26 European countries from the reported confirmed cases from February 24, 2020 (*21*). From these data, we extract the new confirmed cases as the difference between the today's and yesterday's confirmed cases. We sample all European air traffic data from the Eurocontrol dashboard, a pan-European Organization dedicated to support European aviation (*22*). We normalize all air traffic data by the mean traffic from 15 January to 15 February 2020. To estimate the global mobility between different European countries, we employ the annual passenger air travel data (*24*) that represent the travel frequency between two countries. We approximate the individual local mobility using Apple's database from Apple Maps on user's devices. These data represent the relative volume of location requests per country, region, subregion or city, scaled by the baseline volume on 13 January 2020 (*23*). We smoothen the weekday-weekend fluctuations in outbreak and mobility data by applying a moving averaging window of seven days. We analyze the data from the country-specific first day of the outbreak on which 100 infected individuals are reported in each of the 26 European countries as illustrated in Fig. S3.

Local epidemiology modeling

We model the local epidemiology of the COVID-19 outbreak using an SEIR model with four compartments, the susceptible, exposed, infectious, and recovered populations, governed by a set of ordinary differential equations (*27*),

$$\begin{array}{rcccccc} \dot{S} &=& -\beta(t)\,S\,I & & & & \\ \dot{E} &=& +\beta(t)\,S\,I & - & \alpha\,E & & \\ \dot{I} &=& & + & \alpha\,E & - & \gamma\,I \\ \dot{R} &=& & & & + & \gamma\,I\,. \end{array} \tag{1}$$

The transition rates between the four compartments, $\beta(t)$, α, and γ are inverses of the contact period $B(t) = 1/\beta(t)$, the latent period $A = 1/\alpha$, and the infectious period $C = 1/\gamma$. We interpret the latent and infectious periods A and C as disease-specific, and the contact period $B(t)$ as behavior specific. Using the dynamic contact period $B(t)$, we calculate the effective reproduction number $R(t) = C/B(t)$ as an important measure to quantify the current outbreak dynamics.

Global network modeling

We model global mobility using European passenger air travel within a weighted undirected graph $\mathcal{G}$ with $N = 26$ nodes and $E = 201$ edges. The nodes represent the individual countries, the edges the most traveled connections between them. We weight the edges by the estimated annual incoming and outgoing passenger air travel statistics (*24*) from which we create the adjacency matrix, A_{JK}, that represents the travel frequency between two countries J and K, and the degree matrix,

$$D_{JJ} = \text{diag} \sum_{K=1,K\neq J}^{N} A_{JK}\,, \tag{2}$$

that represents the number of incoming and outgoing passengers for each country J. The difference between the degree matrix D_{JK} and the adjacency matrix A_{JK} defines the weighted graph Laplacian (*18, 26*),

$$L_{JK} = D_{JK} - A_{JK}\,. \tag{3}$$

Fig. 1(b) illustrates the discrete graph $\mathcal{G}$ of the European Union with $N = 26$ nodes and 201 edges. The size and color of the nodes represent the degree D_{JJ}, the thickness of the edges represents the adjacency A_{JK}. For our passenger travel-weighted graph, the degree ranges from 222 million in Germany, 221 million in Spain, 162 million in France, and 153 million in Italy to just 3 million in Estonia and Slovakia, and 2 million in Slovenia, with a mean degree of $\bar{D}_{JJ} = 48 \pm 64$ million per node. To calculate the weighted Laplacian L_{JK},

we use the air travel data across the European countries and the United Kingdom (*24*) normalize it such that its largest coefficient is equal to one, and then scale it with the air mobility coefficient ϑ. We discretize our SEIR model on our weighted graph $\mathcal{G}$ and introduce the susceptible, exposed, infectious, and recovered populations S_J, E_J, I_J, and R_J as global unknowns at the $J = 1, ..., N$ nodes of the graph $\mathcal{G}$. This results in the spatial discretization of the set of equations with $4\,N$ unknowns,

$$\begin{aligned}
\dot{S}_J &= -\,\vartheta \textstyle\sum_{K=1}^{N} L_{JK}\, S_K \,-\, \beta\, S_J\, I_J \\
\dot{E}_J &= -\,\vartheta \textstyle\sum_{K=1}^{N} L_{JK}\, E_K + \beta\, S_J\, I_J - \alpha\, E_J \\
\dot{I}_J &= -\,\vartheta \textstyle\sum_{K=1}^{N} L_{JK}\, I_K \qquad\qquad + \alpha\, E_J - \gamma\, I_J \\
\dot{R}_J &= -\,\vartheta \textstyle\sum_{K=1}^{N} L_{JK}\, R_K \qquad\qquad\qquad + \gamma\, I_J\,.
\end{aligned} \tag{4}$$

This continuous dynamical system is coarse-grained in time and replaced by a discrete dynamical system obtained as the one-step Euler discretization of the equations. The resulting fully-discrete system, taken with a step of one day, has the same qualitative behavior as the continuous one and can be easily integrated and updated with daily reporting.

Human mobility modeling

It is useful to capture the general trend of mobility through simple mathematical expression so that they can be easily integrated within the epidemiological model. Here, we introduce a simple ansatz for the global and local mobility. The early phases of the outbreak are characterized by a smooth mobility transition from the initial baseline mobility to a reduced mobility induced by behavioral changes in the population. Previously, we have modeled this transition by a hyperbolic tangent-type ansatz (*27*). Here we generalize this approach by taking into account policy relaxations and social adaptations through a combination of exponentials,

$$y(t) = \frac{y_0\, e^{-(t-t^*)/T} + P(t)\, e^{(t-t^*)/T}}{e^{-(t-t^*)/T} + e^{(t-t^*)/T}} \quad \text{with} \quad y(t) \underset{t\to-\infty}{\sim} y_0 \quad \text{and} \quad y(t) \underset{t\to\infty}{\sim} P(t), \tag{5}$$

where y_0 denotes the baseline value, t^* is the adaptation time, T is the transition time, and $P(t)$ is the adaptation after the initial drop. For the global mobility, European air traffic dropped to a constant plateau of 5% until the end of May 2020, and we select a constant $P(t)$ to model this plateau, see Fig. 1(a). For the local mobility, driving mobility steadily increased after an initial drop at the end of March 2020, and we select a quadratic polynomial $P(t)$ to represent this increase, see Fig. 1 (a). We assume that the the effective

reproduction number follows these mobility patterns, we apply the same functional relation for the effective reproduction number,

$$R(t) = \frac{R_0\, e^{-(t-t^*)/T} + R_t(t)\, e^{(t-t^*)/T}}{e^{-(t-t^*)/T} + e^{(t-t^*)/T}}. \tag{6}$$

This functional form describes a smooth transition from the basic reproduction number R_0 at the beginning of the outbreak to the current reproduction number R_t. We model the effect of the individual mobility on the outbreak dynamics after the initial mobility drop by postulating that the current reproduction number (6) is a function of the time-varying individual mobility $R_t = f[x_{\mathrm{m}}(t)]$. To keep our mobility model simple, interpretable, and capable of handling real-world data, we adopt a stochastic process approach to define $R_t(x_{\mathrm{m}}[t])$ and construct a Gaussian process latent variable model. The Gaussian process model can be considered as a prior distribution for the mapping function (*28*),

$$R_t(x_{\mathrm{m}}) \sim \mathcal{GP}\left\{\mu(x_{\mathrm{m}}), k\left[x_{\mathrm{m}}, x'_{\mathrm{m}}\right]\right\}, \tag{7}$$

which draws function values from a multivariate normal distribution, parameterized by the mean function $\mu(x_{\mathrm{m}})$ and the covariance function $k\left[x_{\mathrm{m}}, x'_{\mathrm{m}}\right]$, while assuming $R_t(x_{\mathrm{m}})$ to be constant within a time window of two days. To account for a smooth non-linear mapping from the latent to the data space, we choose an exponentiated quadratic form covariance function with the two kernel hyperparameters η^2 and ℓ^2 (*29, 30*). A powerful way to stabilize time-series predicting models is to enable trend changes at learned time points S with the aid of weakly informative priors (*31*). These change points can be at any given time point s_j with $j = 1, 2, ..., S$. Here we apply a simple piece-wise linear trend change in the mean function (*31*),

$$\mu(x_{\mathrm{m}}[t]) = \left[k + \boldsymbol{a}(t)^{\mathrm{T}}\boldsymbol{\delta}\right] t + m\left[m + \boldsymbol{a}(t)^{\mathrm{T}}\boldsymbol{\xi}\right] \quad \text{with} \quad a_j(t) = \begin{cases} 1 & \text{if } t \geq s_j \\ 0 & \text{otherwise,} \end{cases} \tag{8}$$

where m is the offset, $\boldsymbol{\delta}$ is the rate adjustment, k is the growth rate, and $\boldsymbol{\gamma}$ enforces continuity as $\xi_j = -s_j\delta_j$.

Bayesian parameter inference

We need to estimate a set of 12 parameters including a set of four parameters for the local SEIR model, $\boldsymbol{\theta}_{\mathrm{SEIR}} = \{\alpha, \gamma, E_0, I_0\}$, a set of seven parameters for the semi-parameteric model, $\boldsymbol{\theta}_{\mathrm{Rt}} = \{t^*, T, \eta^2, \ell^2, k, m, \boldsymbol{\delta}\}$, and one parameter for the network model $\vartheta(t)$. We estimate the mobility parameter $\vartheta(t)$ by fitting (5) against the aviation data in Fig. 1(a) and multiplying it with a scaling prior ϑ_0. We assume that two parameters of the

SEIR model, the latency and infectious periods, $A = 2.5$ and $C = 6.5$, are disease-specific and constant (*32–34*). We estimate the remaining set of model parameters $\boldsymbol{\theta} = \boldsymbol{\theta}_{\mathrm{SEIR}} \cup \boldsymbol{\theta}_{\mathrm{Rt}} \cup \{\vartheta_0\}$ using Bayesian inference with Markov Chain Monte Carlo sampling. We adopted a Student's t-distribution for the likelihood between the model predictions and data (*35, 36*), with a confirmed-case-number-dependent width,

$$p\left(\hat{D}(t)\,|\boldsymbol{\theta}\right) \sim \mathrm{StudentT}_{\nu=4}\left(\mathrm{mean} = D(t,\boldsymbol{\theta}), \mathrm{width} = \sigma\sqrt{\mathrm{D(t,\boldsymbol{\theta})}}\right). \tag{9}$$

Here σ represents the width of the likelihood $p(\hat{D}(t)\,|\,\boldsymbol{\theta})$ between the time-varying reported new cases $\hat{D}(t)$ and the associated modeled $D(t,\boldsymbol{\theta})$ new cases. We apply Bayes' rule to obtain the posterior distribution of the parameters on the basis of the prior distributions specified in Table S1, and the reported cases themselves,

$$p\left(\boldsymbol{\theta}\,|\,\hat{D}(t)\right) = \frac{p\left(\hat{D}(t)\,|\,D(t,\boldsymbol{\theta})\right)\,p(\boldsymbol{\theta})}{p\left(\hat{D}(t)\right)}, \tag{10}$$

which we infer approximately by employing the NO-U-Turn sampler (NUTS) (*37*) implementation of the Python package PyMC3 (*38*). To account for variability between the individual countries, while simultaneously taking advantage of the entire dataset, we adopt a hierarchical model to learn the effective reproduction number on the basis of the case and mobility data. We postulate that during the initial phase, the effective reproduction number is primarily governed by the local political action in each country, while during the later phases, it becomes strongly correlated with local mobility that mimics the new levels of social awareness. We apply hierarchical priors on the parameters of the initial phase, i.e., the basic reproduction number R_0, and the adaptation and transition times t^* and T, and define shared priors on the semi-parametric Gaussian process latent model of the later phases. For each county i, we draw R_{0i} and t_i^* from normal distributions, $R_{0i} \sim \mathcal{N}_i(R_{0i}, \sigma_{R_0})$ and $t_i^* \sim \mathcal{N}_i(t_i^*, \sigma_{t^*})$, and T_i from a log-normal distribution, $T_i \sim \mathcal{N}_i(T, \sigma_T)$, and model the hyper standard deviation priors by half-normal distributions. We design the Gaussian process latent variable model with shared priors for all countries and inform it by the time-varying local mobility data. Here we make use of two hyperparameters for the kernel functions η^2 and ℓ^2. For the forecasting models, we construct a linear-piece-wise means functions defined by three parameters drawn from normal distributions to stabilize the predictive capabilities. W select three equidistant change points, $S = 3$, for the piece-wise linear function. For the network model, we include one additional weakly informative prior for the scaling of the travel coefficient as a normal distribution $\vartheta_0 \sim \mathcal{N}_i(0.4, 0.3)$. Table S1 summarizes all priors on the model parameters.

Acknowledgements

This work was supported by a Stanford Bio-X IIP seed grant to Ellen Kuhl, by a DAAD Fellowship to Kevin Linka, and by the Engineering and Physical Sciences Research Council grant EP/R020205/1 to Alain Goriely.

References

1. J. Zhang, M. Litvinova, Y. Liang, Y. Wang, W. Wang, S. Zhao, Q. Wu, S. Merler, C. Viboud, A. Vespignani, M. Ajelli, H. Yu. Changes in contact patterns shape the dynamics of the COVID-19 outbreak in China. Science (2020) doi:10.1126/science.abb8001

2. L. Goscé, D. Barton, A. Johansson. Analytical modelling of the spread of disease in confined and crowded spaces Scientific Reports 4 (2014) 4856

3. A. Kucharski, T.W. Russel, C. Diamond, Y. Liu, J. Edmunds, S. Funk, R.M. Eggo, F. Sun, M. Jit, J.D. Munday and others Early dynamics of transmission and control of COVID-19: a mathematical modelling study. The Lancet Infectious Diseases (2020 doi:https://doi.org/10.1016/S1473-3099(20)30144-4)

4. X. Pan, D. Cheng, Y. Xia, X. Wu, T. Li, X. Ou, L. Zhou, J. Liu. Asymptomatic cases in a family cluster with SARS-CoV-2 infection. The Lancet Infectious Diseases 20 (2020) 410-411

5. M.U. Kraemer, C.-H.Yang, B. Gutierrez,C.-H. Wu, B. Klein, D. Pigott, L. du Plessis, N.R. Faria, R. Li, W.P. Hanage, J.S. Brownstein, M. Layan, A. Vespignani, H. Tian, C. Dye, O.G. Pybus, S.V. Scarpino. The effect of human mobility and control measures on the COVID-19 epidemic in China Science 368 (2020) 493-497

6. K.E. Ainslie, C.E. Walters, H. Fu, S. Bhatia, H. Wang, X. Xi, M. Baguelin, S. Bhatt, A. Boonyasiri, O. Boyd and others. Evidence of initial success for China exiting COVID-19 social distancing policy after achieving containment. Wellcome Open Research 5 (2020) 81

7. M. Chinazzi, J.T. Davis, M. Ajelli, C. Gioannini, M. Litvinova, S. Merler, A. Pastore y Piontti, K. Mu, L. Rossi, K. Sun, C. Viboud, X. Xiong, H. Yu, M.E. Halloran, I.M. Longini, A. Vespignani. The effect of travel restrictions on the spread of the 2019 novel coronavirus (COVID-19) outbreak. Science 368 (2020) 395-400

8. A. Aleta, D. Martin-Corral, A. Pastore y Piontti, M. Ajelli, M. Litvinova, M. Chinazzi, N.E. Dean, M.E. Halloran, I.M Longini, S. Merler, A. Pentland, A. Vespignani, E. Moro, Y. Moreno. Modeling the impact of social distancing, testing, contact tracing and household quarantine on second-wave scenarios of the COVID-19 epidemic. medRxiv (2020) doi:10.1101/2020.05.06.20092841

9. H. Unwin, S. Mishra, V. Bradley, A. Gandy, M. Vollmer, T. Mellan, H. Coupland, K. Ainslie, C. Whittaker, J. Ish-Horowicz and others. Report 23: State-level tracking of COVID-19 in the United States. Preprint (2020) doi:10.25561/79231

10. S. Gao, J. Rao, Y. Kang, Y. Liang, J. Kruse. Mapping county-level mobility pattern changes in the United States in response to COVID-19 SIGSPATIAL Special 12 (2020) 16-26

11. N. Oliver, B. Lepri, H. Sterly, R. Lambiotte, S. Delataille, M. De Nadai, E. Letouzé, A. Salah, R. Benjamins, C. Cattuto, V. Colizza, N. de Cordes, S. Fraiberger, T. Koebe, S. Lehmann, J. Murillo, A. Pentland, P. Pham, F. Pivetta, J. Saramäki, S. Scarpino, M. Tizzoni, Michele S. Verhulst, P. Vinck. Mobile phone data for informing public health actions across the COVID-19 pandemic life cycle Science Advances (2020) doi:10.1126/sciadv.abc0764

12. R.N. Thompson. Epidemiological models are important tools for guiding COVID-19 interventions. BMC Medicine 104 (2020) 152

13. R. Parshani, S. Carmi, S. Havlin. Epidemic Threshold for the Susceptible-Infectious-Susceptible Model on Random Networks. Physical Review Letters 104 (2010) 258–701

14. B.F. Maier, D. Brockmann. Effective containment explains subexponential growth in recent confirmed COVID-19 cases in China Science 368 (2020) 742–746

15. L. Hufnagel, D. Brockmann, T. Geisel. Forecast and control of epidemics in a globalized world Proceedings of the National Academy of Sciences 101 (2004) 15124–15129

16. M. Enserink, K. Kupferschmidt With COVID-19, modeling takes on life and death importance Science 367 (2020) 1414–1415

17. H. Streeck, B. Schulte, B.M. Kümmerer, E. Richter, T. Höller, C. Fuhrmann, E. Bartok, R. Dolscheid, M. Berger, L. Wessendorf, M. Eschbach-Bludau, A. Kellings, A. Schwaiger, M. Coenen, P. Hoffmann, B. Stoffel-Wagner, M.M. Nöthen, A.M. Eis-Hübinger, M. Exner2, R.M. Schmithausen, M. Schmid, G. Hartmann. Infection fatality

rate of SARS-CoV-2 infection in a German community with a super-spreading event. medRxiv doi:10.1101/2020.05.04.20090076.

18. K. Linka, M. Peirlinck, F. Sahli Costabal, E. Kuhl. Outbreak dynamics of COVID-19 in Europe and the effect of travel restrictions. Computer Methods in Biomechanics and Biomedical Engineering (2020) in press; doi:10.1080/10255842.2020.1759560.

19. S. Flaxman, S. Mishra, A. Gandy, J.T. Unwin, H. Coupland, T.A. Mellan, H. Zhu, T. Berah, J.W Eaton, P. Guzman, N. Schmit, L. Callizo, and Imperial College COVID-19 Response Team. Estimating the number of infections and the impact of non-pharmaceutical interventions on COVID-19 in European countries: technical description update. arXiv (2020) doi:arXiv:2004.11342

20. K. Kwok, F. Lai, W. Wei, S. Wong, J.W.T Tang. Herd immunity–estimating the level required to halt the COVID-19 epidemics in affected countries. Journal of Infection 80 (2020) e32–e33

21. European Centre for Disease Prevention and Control - Covid-19 situation update worldwide. `https://www.ecdc.europa.eu/en/geographical-distribution-2019-ncov-cases`. accessed: 2020-06-03

22. EUROCONTROL - Aviation Data. `https://ansperformance.eu/data/`. accessed: 2020-05-24

23. Apple Mobility Trends. `https://www.apple.com/covid19/mobility`. accessed: 2020-06-03

24. Eurostat(2020). `https://ec.europa.eu/eurostat`. accessed: 2020-04-13

25. H. W. Hethcote. The mathematics of infectious diseases. SIAM Review 42 (2000) 599-653.

26. M. Peirlinck, K. Linka, F. Sahli Costabal, E. Kuhl. Outbreak dynamics of COVID-19 in China and the United States. Biomechanics and Modeling in Mechanobiology (2020) in press, doi:10.1101/2020.04.06.20055863.

27. K. Linka, M. Peirlinck, E. Kuhl. The reproduction number of COVID-19 and its correlation with public health interventions. medRxiv doi:10.1101/2020.05.01.20088047.

28. C.E. Rasmussen. Gaussian processes in machine learning. Summer School on Machine Learning (2003) 63-71

29. M.G. Genton. Classes of kernels for machine learning: a statistics perspective Journal of Machine Learning Research 2 (2001) 299-312

30. N. Lawrence. Probabilistic non-linear principal component analysis with Gaussian process latent variable models. Journal of Machine Learning Research 6 (2005) 1783–1816

31. S.J. Taylor, B. Letham. Forecasting at scale. The American Statistician 72 (2018) 37-45

32. Q. Li, X. Guan, P. Wu, X. Wang, L. Zhou, Y. Tong, R. Ren, K.S.M. Leung, E.H.Y. Lau, J.Y. Wong, X. Xing, N. Xiang, Y. Wu, C. Li, Q. Chen, D. Li, T. Liu, J. Zhao, M. Liu W. Tu, C. Chen, L. Jin, R. Yang, Q. Wang, S. Zhou, R. Wang, H. Liu, Y. Luo, Y. Liu, G. Shao, H. Li, Z. Tao, Y. Yang, Z. Deng, B. Liu, Z. Ma, Y. Zhang, G. Shi, T.T.Y. Lam, J.T. Wu, G.F. Gao, B.J. Cowling, B. Yang, G.M. Leung, Z. Feng. Early transmission dynamics in Wuhan, China, of novel coronavirus-infected pneumonia. New England Journal of Medicine 382 (2020) 1199-1207.

33. S. A. Lauer, K. H. Grantz, Q. Bi, F. K. Jones, Q. Zheng, H. R. Meredith, A. S. Azman, N. G. Reich, J. Lessler. The incubation period of coronavirus disease 2019 (COVID-19) from publicly reported confirmed cases: estimation and application. Annals of Internal Medicine (2020) doi:10.7326/M20-0504.

34. S. Sanche, Y.T. Lin, C. Xu, R. Romero-Severson, N. Hengartner, R. Ke. High contagiousness and rapid spread of severe acute respiratory syndrome coronavirus 2. Emerging Infectious Disease (2020) doi:10.3201/eid2607.200282

35. J. Dehning, J. Zierenberg, F.P Spitzner, M. Wibral, J.P. Neto, M. Wilczek, V. Priesemann. Inferring COVID-19 spreading rates and potential change points for case number forecasts Science (2020) doi: 10.1126/science.abb9789

36. K.L. Lange, R.J.A. Little, M.G. Taylor. Robust statistical modeling using the t distribution. Journal of the American Statistical Association 84 (1989) 881-896.

37. M.D. Hoffman, A. Gelman. The No-U-Turn sampler: adaptively setting path lengths in Hamiltonian Monte Carlo. Journal of Machine Learning Research (2014), 15(1), 1593-1623.

38. J. Salvatier, T.V. Wiecki, C. Fonnesbeck. Probabilistic programming in Python using PyMC3. Peer Journal Computational Science 2 (2016) e55.

Supplementary Material

Supplementary figures

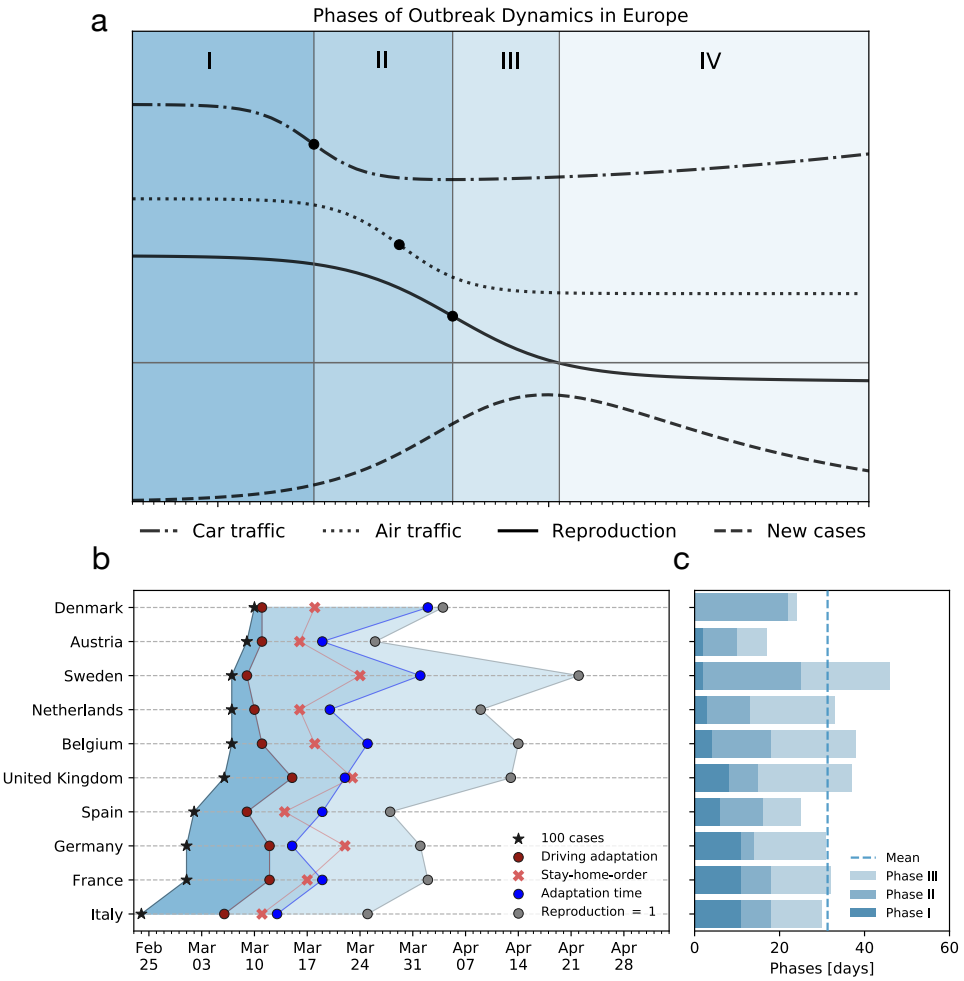

Figure S1: **Schematic & country-specific stages.** (a) Phase I is the disease outbreak and is characterized by a typical exponential growth of new cases. In Phase II, global mobility is quickly reduced. In the lockdown phase III, both local and global mobility are reduced until the number of cases appears to decrease. In Phase IV, lockdown measures are relaxed and mobility increases again. Note that R does not go back to its initial value since many behavioral measures are still in place. The absolute and relative sizes of these different phases depend on the particular social and political organizations of each geographic entities (states or countries). (b) The stage evolution for 10 different European countries is visualized stating at the date where 100 cases have been reported. (c) The bar plot shows the associated duration of the individual phases. The dashed-line indicates the mean duration [31 ± 8 days] of a country to reach $R(t) = 1$ after 100 cases have been recorded. Phase I has a duration of 6 ± 4, phase II of 11 ± 7 and phase III of 14 ± 7 days.

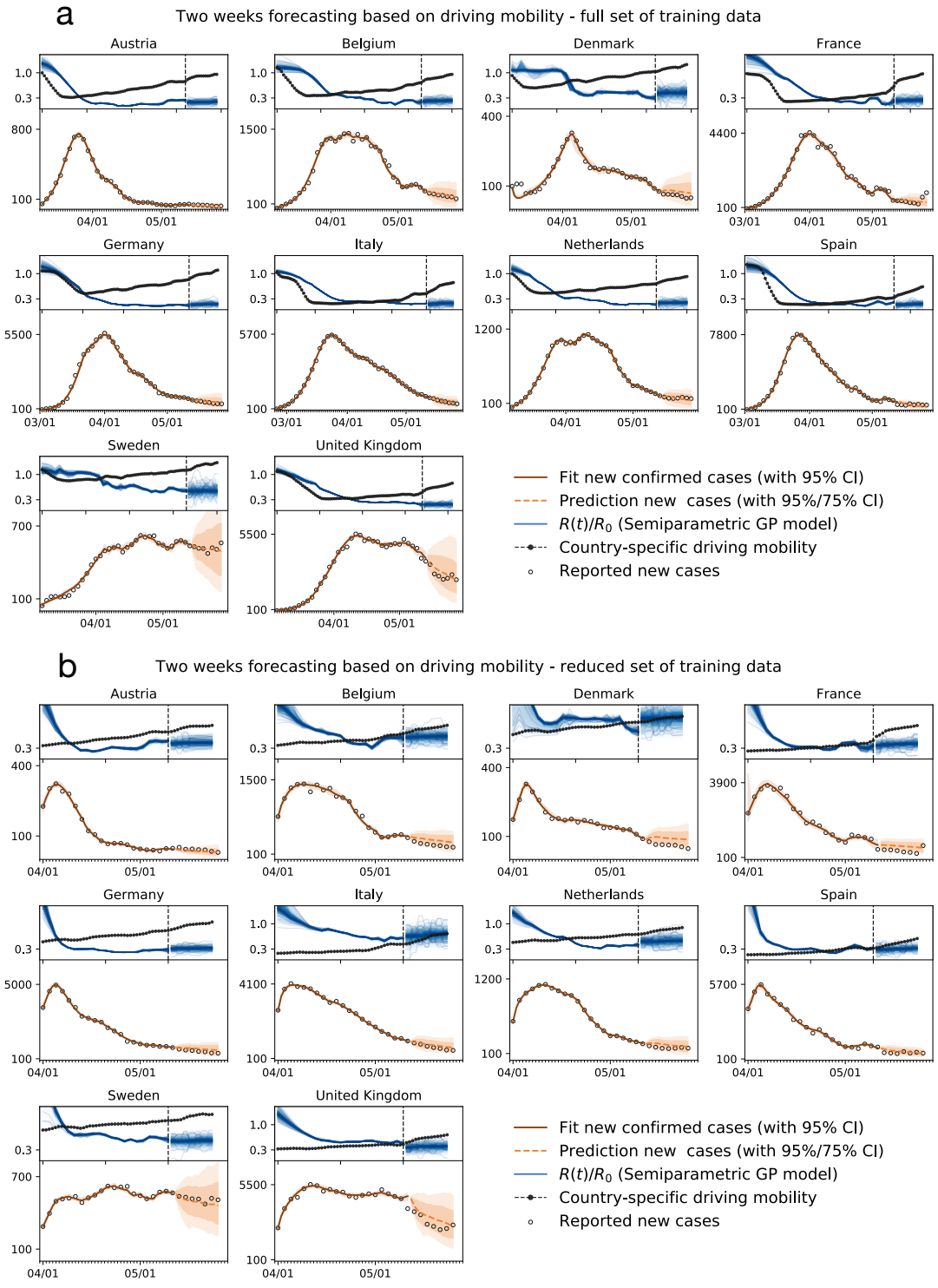

Figure S2: **Two weeks forecasting.**(a) For training the model on the full available data set and (b) training the model on a dataset beginning from 1st of April.

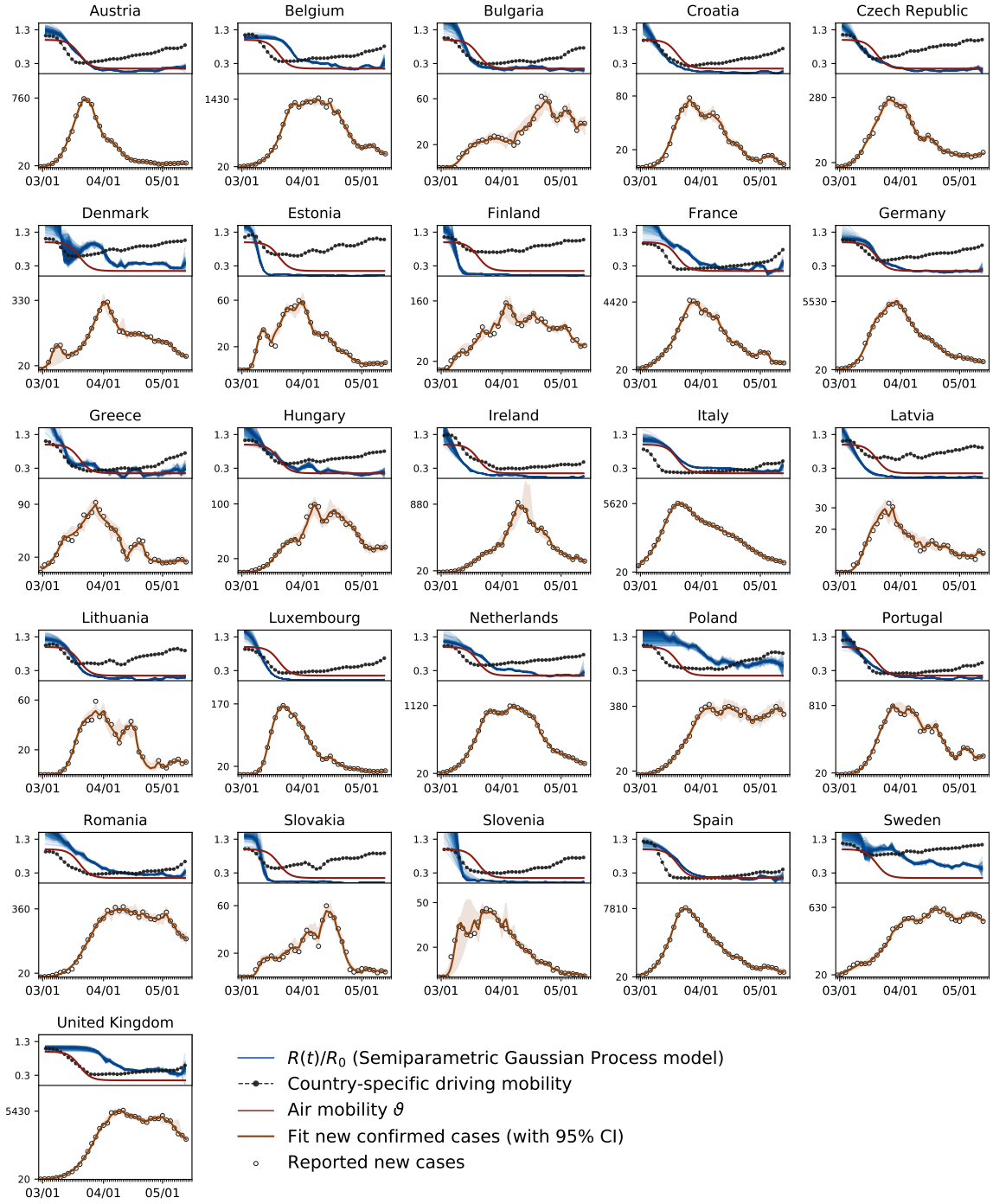

Figure S3: **EU network model results.** The top row of each subfigure shows the learned effective reproduction number vs. the individual driving mobility and global air traffic reduction. Below are the county-specific case data and associated fitting results presented. The data start on 29 February.

Supplementary tables

Table S1: **Priors on the semi-parametric (network) model parameters.**

Parameter	**Variables**	**Prior distributions**
R_0	basic reproduction	Normal(2, 1.5)
σ_{R_0}	std basic reproduction	HalfNormal(1.5)
t^*	adaptation time	Normal(14, 14)
σ_{t^*}	std adaptation time	HalfNormal(15)
T	transition time	LogNormal(log(3), 0.8)
σ_T	std transition time	HalfNormal(0.8)
ℓ^2	hyperparameter	Gamma(2, 0.1)
η	hyperparameter	HalfCauchy(0.5)
k	growth rate	Normal(1, 1)
m	offset	Normal(1, 1)
$\boldsymbol{\delta}$	rate adjustment	Normal(0, 2, shape=S)
I_0	initial infected	LogNormal(log[$\hat{D}(t=0)$], 1.0)
E_0	initial exposed	LogNormal(log[$\hat{D}(t=3)$], 1.0)
ϑ_0	travel coefficient	Normal(0.4,0.3)
σ	likelihood width	HalfCauchy($\beta=1$)